nature structural & molecular biology

Open-ringed structure of the Cdt1–Mcm2–7 complex as a precursor of the MCM double hexamer

Yuanliang Zhai[1,2,6], Erchao Cheng[3,6], Hao Wu[3], Ningning Li[4], Philip Yuk Kwong Yung[1], Ning Gao[3] & Bik-Kwoon Tye[1,5]

The minichromosome maintenance complex (MCM) hexameric complex (Mcm2–7) forms the core of the eukaryotic replicative helicase. During G1 phase, two Cdt1–Mcm2–7 heptamers are loaded onto each replication origin by the origin-recognition complex (ORC) and Cdc6 to form an inactive MCM double hexamer (DH), but the detailed loading mechanism remains unclear. Here we examine the structures of the yeast MCM hexamer and Cdt1–MCM heptamer from *Saccharomyces cerevisiae*. Both complexes form left-handed coil structures with a 10–15-Å gap between Mcm5 and Mcm2, and a central channel that is occluded by the C-terminal domain winged-helix motif of Mcm5. Cdt1 wraps around the N-terminal regions of Mcm2, Mcm6 and Mcm4 to stabilize the whole complex. The intrinsic coiled structures of the precursors provide insights into the DH formation, and suggest a spring-action model for the MCM during the initial origin melting and the subsequent DNA unwinding.

DNA replication in eukaryotes is strictly regulated to ensure perpetuation of the integrity of the genome[1,2]. To ensure that each replication origin is activated no more than once per cell division, the initiation of DNA replication is carried out in two temporally separated steps: replication licensing, and origin activation[3]. Replication licensing begins in early G1 phase with the sequence-specific binding of origin DNA by the ORC (Orc1–6) to first recruit Cdc6 and then other factors[3]. Escorted by Cdt1 (ref. 4), the MCM single hexamer (SH)[5–7] is loaded onto the ORC–Cdc6-bound origin DNA[8–10] to form an ORC–Cdc6–Cdt1–MCM2–7 (OCCM) complex[11–13]. Subsequently an ordered release of Cdc6 and then Cdt1 occurs, leading to the formation of an ORC–Mcm2–7 complex[14]. The loading of a second Mcm2–7 is not yet fully understood but also involves the incorporation of Cdt1, Cdc6 and ORC[14] to complete the assembly of a head-to-head Mcm2–7 DH known as the pre-replication complex (pre-RC)[8,9,15,16]. The pre-RC lacks helicase activity until the cell enters S phase[8]. At the transition from G1 to S phase, two kinases, Dbf4-dependent kinase (DDK) and S-phase-specific cyclin-dependent kinase (S-CDK), act in concert with multiple helicase-activating factors to transform the inert DH into two active Cdc45–Mcm2–7–GINS (CMG) helicases[17–19]. Phosphorylation of Mcm2–7 by DDK[20,21] enables the sequential loading of Sld3, Sld7 and Cdc45 (refs. 22,23), whereas phosphorylation of Sld3 and Sld2 by CDK[24,25] facilitates the loading of Sld2, GINS, Dpb11 and other factors to form the pre-initiation complex[18,26,27]. Activation of the pre-initiation complex occurs when the DH is separated into two active helicases and DNA polymerase complexes are recruited to the bidirectional replication forks to form two active replisomes[3,28].

Much work has been devoted to the study of the assembly of the pre-RC that licenses replication origins for DNA synthesis using the budding yeast system. Current studies favor the model in which the yeast Mcm2–7 proteins assemble into a closed ring structure that must be loaded onto ORC–Cdc6-bound duplex DNA by means of ring opening at the Mcm2-Mcm5 gate with the help of Cdt1 (refs. 6,29–31). The formation of the DH is an energy-consuming process that requires the binding and hydrolysis of ATP by the MCM ATPase[32,33]. We previously determined the structure of the DH at near-atomic resolution and showed that the two SHs are joined head to head at the N-terminal ends by interactions of their rings of zinc fingers[16]. This dimeric structure is further cemented by the interdigitation of N-terminal extensions (NTEs) and N-terminal insertions (NTIs) of the opposing rings. The elaborate arrangement of the coupling of the two SHs suggest that major conformational changes, especially at the N-terminal domains (NTDs), are involved in the establishment of the tight connection. In archaea, the MCM helicase is a homohexamer and lacks the NTEs and NTIs found in eukaryotes[34]. In these simpler systems, unlike in their eukaryote counterparts, DHs are assembled readily in solution in the absence of DNA[35,36].

To understand more about the elaborate mechanism behind the formation of the DHs in eukaryotes and about the functional design for such tight coupling, we focused on the structures of the precursors of the DH—both Mcm2–7 (hexamer) and Cdt1–Mcm2–7 (heptamer)—before their loading onto DNA.

[1]Division of Life Science, Hong Kong University of Science and Technology, Clear Water Bay, Hong Kong, China. [2]Institute for Advanced Study, Hong Kong University of Science and Technology, Clear Water Bay, Hong Kong, China. [3]Ministry of Education Key Laboratory of Protein Sciences, Beijing Advanced Innovation Center for Structural Biology, School of Life Sciences, Tsinghua University, Beijing, China. [4]Peking-Tsinghua Center for Life Sciences, School of Life Sciences, Peking University, Beijing, China. [5]Department of Molecular Biology and Genetics, College of Agriculture and Life Sciences, Cornell University, Ithaca, New York, USA. [6]These authors contributed equally to this work. Correspondence should be addressed to N.G. (ninggao@tsinghua.edu.cn) or B.-K.T. (biktye@ust.hk).

Received 6 September 2016; accepted 9 January 2017; published online 13 February 2017; doi:10.1038/nsmb.3374

RESULTS

Overall structures of Mcm2–7 and Cdt1–Mcm2–7

First we incubated the purified Mcm2–7 and Cdt1–Mcm2–7 complexes (**Supplementary Fig. 1a–c**) with either nonhydrolyzable ATP analog adenylyl imidodiphosphate (AMPPNP) or adenosine diphosphate (ADP) in large excess to saturate them in different nucleotide-binding states before cryo-electron microscopy (cryo-EM) sample preparation. We acquired data with a Titan Krios microscope equipped with a K2 camera (**Supplementary Fig. 1d** and **Table 1**). Subsequent 2D and 3D classifications and refinements rendered a series of density maps at 7–8-Å resolution (**Supplementary Figs. 1e–g** and **2**). Secondary structures resolved in the maps allowed us to confidently assign each component and to build models for the MCM subunits and Cdt1 (**Fig. 1** and **Supplementary Video 1**).

The most notable feature for all four complexes is that the six MCM subunits are arranged in a very similar, left-handed helical manner, with an obvious gap between Mcm5 and Mcm2 (**Fig. 1** and **Supplementary Fig. 3**). This open ring structure is consistent with low-resolution structures observed previously for the Mcm2–7 hexamers from *Encephalitozoon cuniculi* and *Drosophila melanogaster*[37,38], but it contrasts with the closed ring structure of the yeast hexamer obtained from negative-staining electron microscopy[29]. The discrepancy probably arises from the differences between the two studies in terms of sample homogeneity, image resolution and the number of single particles analyzed. However, the size of the gap is about 10–15 Å—too narrow for double-stranded DNA (dsDNA) to pass through (**Fig. 1i–j**)—which suggests that additional conformational changes that widen the gap have to take place in order for Mcm2–7 to be loaded onto duplex origin DNA.

As major players in the intersubunit interaction in the DH[16], the six oligonucleic-acid-binding subdomains (OBs) also display a spiral arrangement (**Supplementary Fig. 4**). Compared with the DH, the OBs of Mcm4, Mcm7 and Mcm6 in the hexamer and heptamer show little change, whereas that of Mcm3 shows a moderate shift, and those of Mcm5 and Mcm2 undergo the most obvious axial and lateral displacements.

Unique conformations of N-terminal zinc-finger and C-terminal winged-helix motifs

The zinc-finger (ZF) motifs in the hexamer and heptamer are organized in very different orientations, and the inter-ZF distances also vary considerably (**Fig. 2a**,**c**), in contrast to the nearly symmetric arrangement of the ring of six ZFs in the DH[16] (**Fig. 2b**,**d**).

In addition to conserved domains for MCM subunits, we were able to identify and build models for winged-helix (WH) motifs from Mcm5, Mcm4 and Mcm6 (**Fig. 2e–h**). Similar to the CMG complex[39], the WH motif of Mcm5 is situated in the central channel (in the top view) and, together with the narrow gap, blocks dsDNA access to the channel (**Fig. 2e**,**f**). The WH motifs of Mcm6 and Mcm4 next to each other form a pseudo-dimer (**Fig. 2h**) that extends along the channel axis toward the C-terminal end, occupying the most outstanding position of the hexamer (**Supplementary Fig. 3a**,**c**) or the heptamer (**Fig. 2e**,**f**,**h**). This arrangement is in sharp contrast to those observed in the DH and the CMG complex. In the DH, all five of the WH-containing extensions of the MCM subunits (Mcm3–7) are flexible[16], whereas in the CMG complex, only the WH motifs of Mcm5 and Mcm6 can be structurally resolved[39]. This extended WH dimer is at the ORC-interacting interface of the MCM[13], which suggests that conformational rearrangement of these WH motifs is likely to regulate the binding and release of the ORC during the MCM-loading process.

Interaction of Cdt1 with Mcm2–7

Cdt1 is an enigmatic replication factor because it has been shown to interact with multiple replication-initiation factors, including a subset of the MCM subunits[4,30,40–42]. However, the structure of full-length Cdt1 has not been determined. In this study of Cdt1–MCM, we were able to identify three domains of Cdt1, wrapping around the NTDs of Mcm2, Mcm6 and Mcm4 (**Fig. 3a**,**b**). The middle domain (MD) of Cdt1 interacts with the NTD of Mcm2 (**Fig. 3c**). At the Mcm2-Cdt1 interface there is a large piece of unassigned density, which probably represents the structured interaction between Cdt1 and the NTE of Mcm2 (**Fig. 3c**). A flexible linker that was not well resolved in our

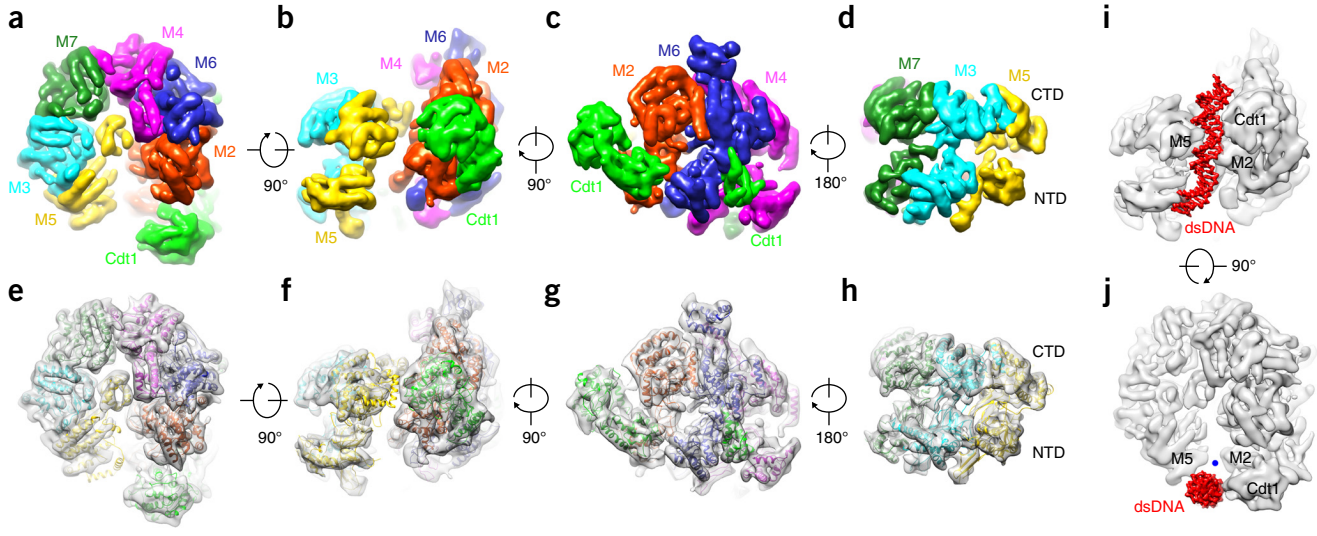

Figure 1 Overall structure of the heptamer saturated with AMPPNP. (**a**–**d**) The cryo-EM map of the Cdt1–MCM complex (AMPPNP-saturated) shown in surface representation, with subunits color-coded as indicated by the labels. Shown are the top (**a**) and side views (**b**–**d**) of the CTD. (**e**–**h**) Same as **a**–**d**, but shown in transparent surface representation, with models superimposed. CTD, C-terminal domain; NTD, N-terminal domain. (**i**,**j**) The Mcm2-Mcm5 gap is not wide enough for dsDNA to pass through; shown in side (**i**) and top view (**j**). The dsDNA model was taken from a previously reported model (PDB 4KFC). DNA is shown in red. The blue dot marks the narrowest point of the gap. M, Mcm.

Table 1 Data-processing statistics

	Heptamer + AMPPNP (EMD-6671)		Heptamer + ADP (EMD-6672)		Hexamer + ADP + 0.005% NP-40
Data collection					
TEM	Titan Krios		Titan Krios		Titan Krios
Camera	K2 Summit		K2 Summit		K2 Summit
Pixel size (Å)	1.32		1.32		1.32
Image processing					
Micrographs (original micrographs)	2,191 (2,848)		2,029 (2,746)		1,580 (2,074)
Box size (pixels)	200		200		160
Particles for 2D classification	402,000		416,000		374,000
Particles for 3D classification	244,400		283,000		224,000
Particles for 3D refinement	63,000	51,800	47,200	42,300	41,500
Complex state	Heptamer–AMPPNP	Hexamer–AMPPNP	Heptamer–ADP	Hexamer–ADP[a,b]	Hexamer–ADP[b,c]
Final resolution (Å)	7.1	8.0	7.1	8.0	7.3

[a]The Heptamer + ADP data are from carbon-coated holey grids. [b]The two structures of the hexamer–ADP complex were similar, and only the one with higher resolution was used for structural analysis. [c]The Hexamer + ADP + NP-40 data were from holey grids. TEM, transmission electron microscope.

study presumably wraps around the NTD of Mcm6 (**Fig. 3b**) and lodges the Cdt1 C-terminal domain (CTD) in a position where it is surrounded by the Mcm6 NTD, the Mcm6 N-C linker, the Mcm4 N-C linker and the Mcm4 NTD (**Fig. 3d**,**e**). Both the MD and the CTD of Cdt1 contain WH motifs[43] that occupy strategically equivalent positions between the Mcm2 NTD and the Mcm6 NTD, and between the Mcm6 NTD and the Mcm4 NTD, respectively. Notably, the interaction between the NTDs of Mcm6 and Mcm4 is not enhanced by their NTIs, as observed in the DH[16]. By comparing the structures of the SH and the heptamer, and on the basis of the interactions between the NTDs of the MCM subunits and Cdt1 in these regions, we concluded that Cdt1 probably contributes to the stabilization of the Mcm2–7 complex by enhancing intersubunit interactions. We noted that Mcm6 and Mcm4 were the two subunits with the longest and therefore most flexible N-C linkers. The Cdt1 CTD, via its interactions with these N-C linkers, potentially could also contribute to the conformational modulation of the hexameric complex during the dynamic loading process.

Although the Mcm6 N-C linker could not be fully traced, given its apparent difference from that in the DH (**Supplementary Fig. 5**), we believe that Cdt1 binds to the MCM hexamer only when it is in its open-ring conformation. Indeed, if the subunits of Mcm2, Mcm6 and Mcm4 from the DH were aligned to their Cdt1-bound conformations individually, using the Mcm6 NTD as reference, the constellation of Cdt1 binding sites on Mcm2, Mcm4 and Mcm6 could no longer be established (**Supplementary Fig. 5**). Thus, after hexamer loading, the closing or narrowing of the gap would spontaneously release Cdt1 from the Mcm2–7 complex.

In this arrangement, Cdt1 embraces approximately half of the ring around the neck region. However, the NTD of Cdt1, though juxtaposed to the C-terminal AAA+ domain (CTD-A) of Mcm2, has no apparent interaction with it, although when the map was displayed at a very low contour level we could see one weak density connection. Also, the direct interaction observed between the Cdt1 CTD (481–501) and the Mcm6 C-terminal extension (CTE) (897–1,009) by NMR spectroscopy analysis[42] was not observed in our structure. We suspect that transient and dynamic conformational changes in both the MCM subunits and Cdt1 would occur upon contact with ORC–Cdc6.

Intrasubunit conformational changes of individual MCM subunits

We showed previously that in the DH, CTD-As in all six MCM subunits are nearly vertically arranged relative to their respective NTDs along the hexamer axis[16]. Given the coiled structure of the Mcm2–7 complex, intrasubunit (interdomain) orientation changes must have taken place. Alignments of individual MCM subunits from the two complexes revealed that all six subunits had undergone dramatic conformational changes. Specifically, when the CTD-As are used as a reference to align individual subunits, corresponding NTDs must rotate counter-clockwise to assume their positions in the DH (**Fig. 4**). However, the displacement of the NTDs within each MCM subunit is not uniform, and could be as large as 50 Å. Among the six subunits, two gate-forming subunits, Mcm5 and Mcm2, showed the largest changes (r.m.s. deviations of 29 and 31 Å, respectively). This interdomain shift suggests that after hexamer loading and gap closing, the six subunits undergo concerted intrasubunit motion and collectively translate into an inter-ring rotation of the hexamer (**Supplementary Video 1**).

Within the NTDs of MCM subunits, the relative orientation changes of individual subdomains also vary from subunit to subunit. When we aligned the individual NTDs to their counterparts in the DH using subdomain A of the N-terminal domain (NTD-A) as a reference, the ZF motifs of Mcm2 and Mcm3 underwent drastic shifts of up to 20 Å and 10 Å, respectively (**Supplementary Fig. 6a**–**f**), whereas the orientations between the NTD-A and OBs for all six MCM subunits showed minimal changes. Thus the NTDs of all subunits except Mcm2 and Mcm3 are relatively rigid during the loading process.

Intersubunit orientation changes of the MCM heptamer relative to the DH

Previous studies showed that ATPase activity is required for the loading of the MCM hexamer to form the ORC–Cdc6–Mcm2–7 and DH complexes[12,32,33]. We were prompted to examine the ATPase centers in the MCM hexamer with respect to the inactive DH. Aside from the complete disruption of the Mcm5-Mcm2 ATPase center by the gap between them, we observed only subtle changes at the interfaces of the CTD-A that form the five ATP-binding pockets in the open-ringed hexamer or heptamer. As shown in **Supplementary Figure 6g**–**k**, when we used one CTD-A of each neighboring pair as the reference for alignment and calculated the r.m.s. deviation of the other CTD-A in the hexamer and the DH, we observed only minor changes ranging from 4 to 6 Å. Although the resolution of the current structures does not allow us to determine the states of activity for these ATPase centers, the small changes in the CTD-A interfaces suggest that functional ATPase centers are preserved in the hexamer. This finding supports previous data showing that ATPase activity of the MCM subunits is required for DH formation and Cdt1 release[12,32,33].

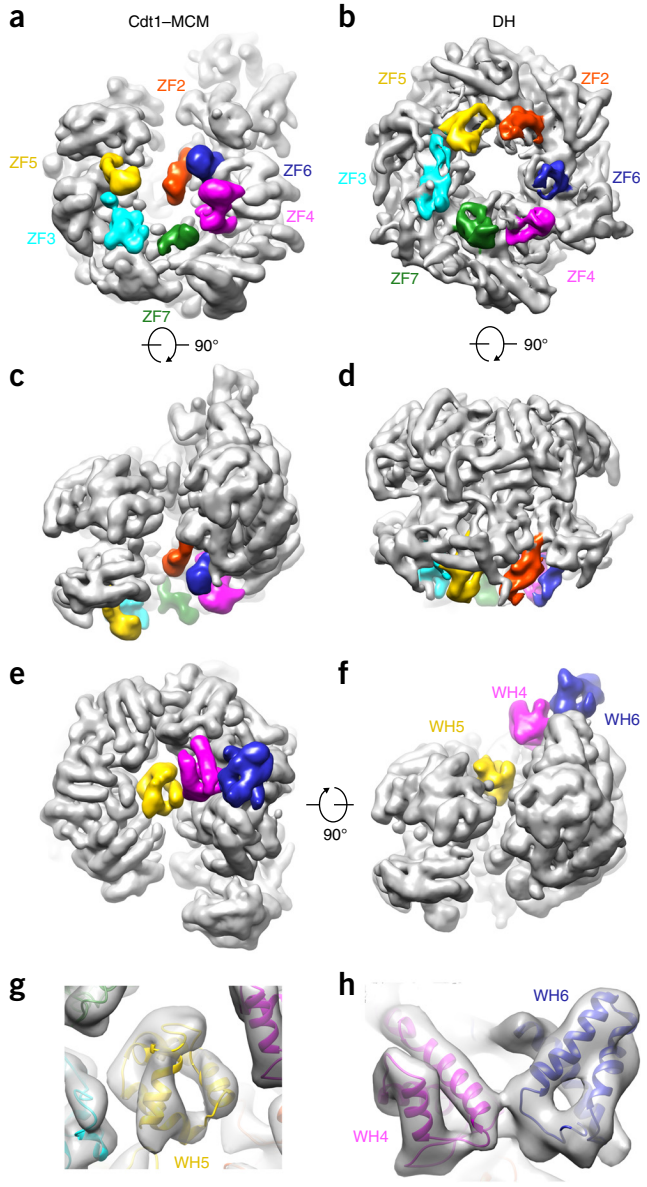

Figure 2 Arrangement of N-terminal ZF and C-terminal WH motifs in the heptamer. (**a**–**d**) Orientations of N-terminal ZFs of the Cdt1–MCM heptamer (**a**,**c**) and in the MCM DH (**b**,**d**). Shown are the bottom (**a**,**b**) and side views (**c**,**d**) of the NTD. The ZFs are color-coded as indicated by the labels. (**e**,**f**) Top (**e**) and side (**f**) views of C-terminal WH motifs of Mcm5 (yellow), Mcm6 (blue) and Mcm4 (magenta) in the heptamer. (**g**,**h**) Zoomed-in views highlighting the WH models of Mcm4, Mcm5 and Mcm6.

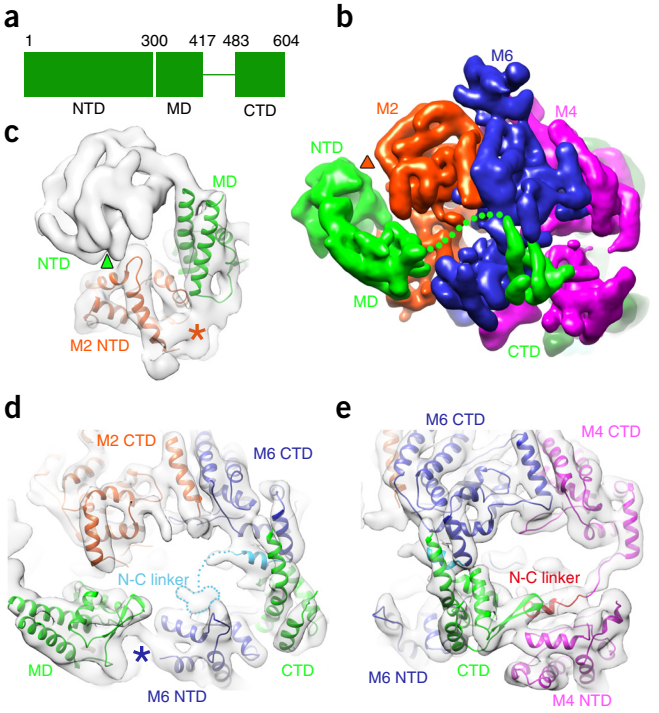

Figure 3 Interaction of Cdt1 with Mcm2–7. (**a**) Schematic representation of the domain organization of Cdt1, with amino acids comprising the NTD, MD and CTD indicated. (**b**) Overview of the interactions between Cdt1 and MCM subunits. The green dotted line indicates a possible path for the flexible M-C linker of Cdt1. Possible weak interaction between the Cdt1 NTD and the Mcm2 CTD is denoted by an orange triangle. (**c**) Zoomed-in view of the interactions between Cdt1 and Mcm2 (M2). The density map (transparent gray) is superimposed on the models of individual components. The unassigned density of the Mcm2 NTE is marked by an orange asterisk. Potential interaction between the Cdt1 NTD and the Mcm2 NTD is denoted by a green triangle. (**d**) Zoomed-in view of the interactions between Cdt1 and Mcm6. A site where the Cdt1 MD makes contact with the unassigned density of the N-terminal insertion of Mcm6 is marked with a blue asterisk. The Mcm6 NTD is sandwiched between the MD and CTD of Cdt1. (**e**) Zoomed-in view of the interactions of the Cdt1 CTD with Mcm6 and Mcm4. Subunits and linkers are color-coded according to the labels. M, Mcm.

Structural comparison of the hexamer and heptamer

The general conformations of the hexamer and heptamer are quite similar, which suggests that Cdt1 is not involved in opening the Mcm2-Mcm5 gate. But there are noticeable differences between the N-terminal regions of the two structures. Although Cdt1 does not make physical contact with Mcm7, Mcm3 or Mcm5, the binding of Cdt1 to Mcm2, Mcm6 and Mcm4 appears to have an allosteric effect on the stability of the NTDs of Mcm7, Mcm3 and Mcm5, with the Mcm7 NTD being affected the most (**Fig. 5a**,**b**). The stabilizing effect of Cdt1 on the Mcm2–7 complex was apparent in the purification of the SH and heptamer on glycerol gradient sedimentation (**Supplementary Fig. 1**). It is also supported by our structural data, which showed that when a similar number of particles was used for 3D structure reconstruction, the overall resolution of the hexameric complex decreased (**Supplementary Fig. 2** and **Table 1**). These observations corroborate the finding that recruitment of the MCM hexamer by ORC–Cdc6 could still occur in the absence of Cdt1 *in vitro*, albeit with much less efficiency[11]. Together, these results suggest that Cdt1 regulates the kinetics of Mcm2–7 loading by stabilizing the SH, rather than by opening the gate.

Nucleotide-dependent conformational transitions of the MCM hexamer

In the present study, we carried out sample purification with excess ATP in the buffer. Given the robust activity of MCM hexamers to hydrolyze ATP[12,29,44], the resulting complexes could be assumed to contain a mixture of ATP and ADP. To produce four distinct functional states for the MCM hexamer, we incubated the hexamers and heptamers with a large excess of either AMPPNP or ADP for 1 h to allow sufficient nucleotide exchange before cryo-freezing. However, these different functional states were not associated with large conformational differences in the overall architecture of the hexamer,

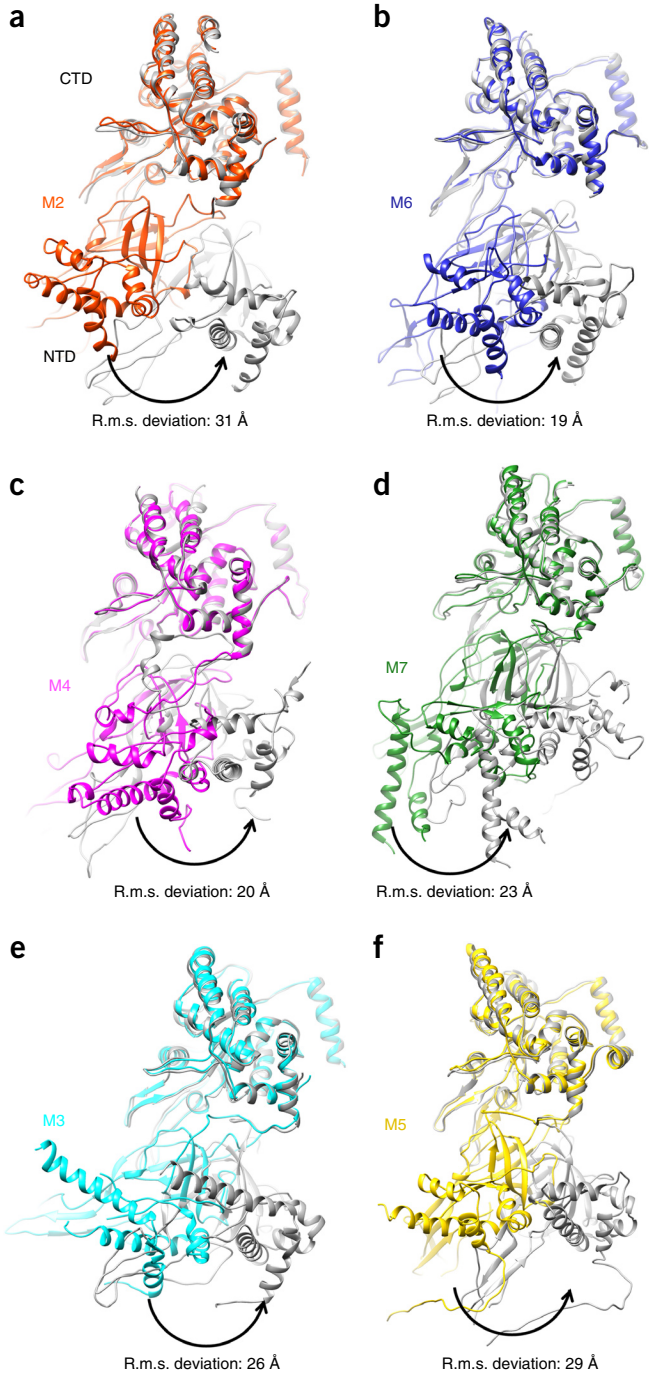

Figure 4 Conformational changes of individual MCM subunits in the heptamer relative to the DH. (**a**–**f**) Superimposed views of individual MCM subunits from the heptamer (color coded according to the labels) and the DH (in gray): (**a**) Mcm2, (**b**) Mcm6, (**c**) Mcm4, (**d**) Mcm7, (**e**) Mcm3 and (**f**) Mcm5. We used the CTD-A of each subunit as a reference for the alignments. The r.m.s. deviation values indicate positional changes of the subunit NTDs. M, Mcm.

although in general the AMPPNP-saturated state seemed to be more stable, particularly in the N-terminal regions (**Fig. 5**). This observation is in agreement with previous work showing that ATPγS stabilizes the structures of both hexamers and heptamers *in vitro*[29,32,37,45]. Given the resolution limitations, we could not carry out a quantitative analysis for these structures, but a previous small-angle X-ray scattering study using *E. cuniculi* Mcm2–7 complex suggested that the ATP binding compacts the hexamer but does not promote gap closure[37]. Notably, the conformational similarity of these structures is consistent with the general model stating that ATP hydrolysis is not required for the dynamic loading process *per se*; rather, it is required for Cdt1 release and further conformational changes that form the DH[32,33]. Together, these results suggest that the nucleotide state of the heptamer is not the limiting factor in determining the conformational status of the MCM for its efficient loading onto origin DNA.

DISCUSSION

Mcm2–7 hexamers are intrinsically open coiled rings

Extensive experimental data have established a model for the stepwise loading of two MCM hexamers to form a DH at the replication origin (reviewed in ref. 3). On the basis of the structures of prototypical homohexameric replicative helicases and translocases from archaea and bacteria[36,46–49], one might expect that the Mcm2–7 hexamer also assumes a closed-ring structure. Loading of these closed-ring structures onto DNA typically requires the aid of a ring loader that opens and closes the ring[50]. A prime example is the bacterial DnaB hexameric ring, which is cracked open by the ring loader DnaC before being loaded onto the DnaA melted single-stranded origin DNA[51].

Recent studies, however, showed several examples of an alternative mechanism for the loading of hexameric MCMs. In these examples, preexisting open-ring structures are loaded onto DNA without the need for a specific ring loader to crack the ring. In the archaea *Sulfolobus islandicus*, temperature plays a critical role in regulating the transition between the open and closed conformations of the MCM ring[52]. Structural studies on MCM hexamers from different species, including *E. cuniculi* and *D. melanogaster*[37,38], showed that they all assume a left-handed open-ring conformation. Our current study is consistent with the alternative mechanism in which both the hexamer and the heptamer also assume a left-handed open-ring conformation. Moreover, the role of Cdt1 in stabilizing a preexisting hexameric open-ring structure is more like that of a chaperone than that of a ring loader that cracks open the ring. However, the gap between Mcm2 and Mcm5 is not wide enough to allow the entry of dsDNA into the central channel. Clearly, further conformational change is necessary to widen the gate for MCM loading. Previous studies showed that ORC–Cdc6 recruits the Cdt1–MCM heptamer onto origin DNA to form the intermediate complex OCCM in the presence of ATPγS[13,29]. At this stage, the CTD-As of the MCM complex have already assumed a closed-ring configuration, encircling dsDNA, whereas the NTDs between Mcm2 and Mcm5 remain separated[13]. This finding suggests that the initial contact between ORC–Cdc6 and Cdt1–MCM may transiently widen the Mcm2-Mcm5 gate and clear the Mcm5 WH from the central channel to allow for loading of the heptamer onto DNA. To a certain extent, the partnership between Mcm2–7 and ORC–Cdc6 is analogous to that of the clamp protein proliferating cell nuclear antigen (PCNA) and its loader complex replication factor C (RFC)[53,54], but with distinct differences. First, unlike PCNA, which forms a closed-ring homotrimer, the heterohexameric Mcm2–7 complex assumes an open coiled structure. Second, the interaction between Mcm2–7 and ORC–Cdc6 occurs only at origin DNA where ORC–Cdc6 is bound, whereas RFC associates with PCNA before loading it onto DNA and breaks the ring. Third, after loading, the clamp loader leaves the PCNA ring encircling DNA, whereas ORC remains associated with Mcm2–7 until after loading of the second MCM hexamer.

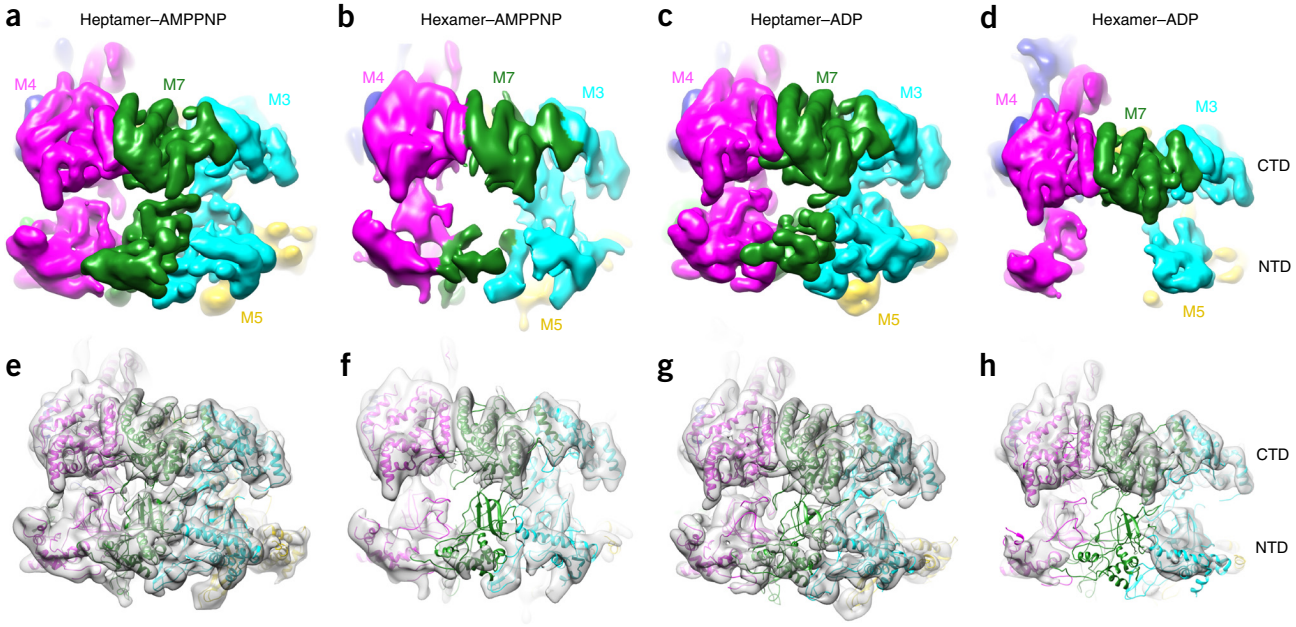

Figure 5 Structural comparison of the AMPPNP- or ADP-saturated heptamers and hexamers. (**a**–**d**) Cryo-EM maps of the heptamer–AMPPNP (**a**), hexamer–AMPPNP (**b**), heptamer–ADP (**c**) and hexamer–ADP (**d**) complexes, shown in surface representation, with individual Mcm3, Mcm4, Mcm5 and Mcm7 subunits color-coded according to the labels. (**e**–**h**) The EM density maps (in transparent gray) with models superimposed for the heptamer–AMPPNP (**e**), hexamer–AMPPNP (**f**), heptamer–ADP (**g**) and hexamer–ADP (**h**) complexes. M, Mcm.

Safeguard against premature loading

An important feature of the ring-loading mechanism is the safeguard against premature loading of the SH. We believe that the narrow Mcm2-Mcm5 gate, the WH domain of Mcm5, and the position of the Cdt1 NTD all serve as safeguards against premature MCM loading. It is interesting to note that Cdc45 and GINS in the CMG complex bind to a planar or near-planar conformation of MCM (NTDs of Mcm3, Mcm5 and Mcm2)[39,55]. Mapping of Cdc45 and GINS on the heptamer indicated that they are not compatible with the MCM in this conformation (**Supplementary Fig. 7a–d**). Steric hindrance is perhaps a means to prevent the premature association of helicase-activating factors before the MCM is loaded onto DNA.

Structure and function of Cdt1

Our heptamer structure shows that Cdt1 can be divided into three globular domains and one flexible linker: the NTD, the MD, the M-C linker and the CTD (**Fig. 3**). The MD and CTD have important roles in stabilizing the NTDs of the hexamer and, most conspicuously, the NTD of Mcm7. The effect of Cdt1 on the NTDs of the MCM hexamer is strikingly similar to that observed for GINS and Cdc45 in the CMG structure[39]. This similarity attests to the intrinsic instability of the hexamer on its own and the fact that it needs accessory proteins in order to carry out its many functions. The instability of the NTDs of the hexamer is perhaps a functional design in partnership with Cdt1. The current model of MCM loading favors the asymmetric loading of two SHs, one at a time[14,15]. Cdt1 loads the first SH at the ORC–Cdc6 binding site as an assembled complex and is then expelled[11,12], leaving a bound SH with a less ordered NTD ring, which might be particularly important for the recruitment of a second SH. The second heptamer is loaded without the need for direct association with the ORC–Cdc6 complex, and the DH forms once Cdt1 is released. We believe that disordered NTDs of both hexameric rings at this crucial moment may be critical for the formation of the tight junction, with elaborate interactions between them (**Fig. 6a**). No additional factor is required for this end-to-end fusion step[8,11,12,14,18], but ATP hydrolysis by the MCM ATPase is required[32,33]. Notably, the most flexible NTD of Mcm7 in the SH makes an important contribution to DH stabilization through its interaction with the NTDs of both Mcm5 and Mcm3 from the opposite hexamer[16]. Thus, Cdt1 might act as a chaperone and orchestrate the fusion of the NTDs between the two SHs.

In addition, the Cdt1 NTD seems to have only weak interactions with Mcm2. Previous studies showed that the DH assembled by Cdt1ΔNTD is defective in recruiting Cdc45 and GINS onto the DH after helicase activation[30]. So the Cdt1 NTD must have some role in remodeling the SH as the heptamer is being loaded onto DNA, perhaps through allosteric interactions between Cdt1 and Cdc6–ORC[41,56]. As for the M-C linker, its extendable flexibility apparently enables the cross-subunit interactions of the MD and CTD with multiple domains of the SH. Notably, a previous study also suggested an interaction of the Cdt1 CTD with the Mcm6 CTE[42]. This flexible linker may become useful again during a later stage, after the initial loading of the hexamer onto chromatin, as it could re-lodge the CTD without compromising the interactions at the MD and NTD.

The significance of the intrinsic open-coil structure of the MCM hexamer

The fact that the precursors of the DH exist as two open-coil springs suggests that during the transition from two SHs to a DH, the two coiled springs will have to be compressed to form two planar rings (**Fig. 6b**). This compression would mean that energy would be stored in the DH, and the process would require energy, as predicted from biochemical and genetic analysis[32,33,57]. Thus, the planar or near-planar configurations of the Mcm2–7 hexamer as observed in the DH[15,16], OCCM[13] or CMG[38,39,55,58] have a tendency to spring wide open. Therefore, additional interactions are required to hold the complex in a closed-ring conformation. For example, extensive N-terminal interactions between the two SHs in the DH, ORC–Cdc6 in OCCM, and Cdc45–GINS in CMG all help to keep the MCM hexamer in a

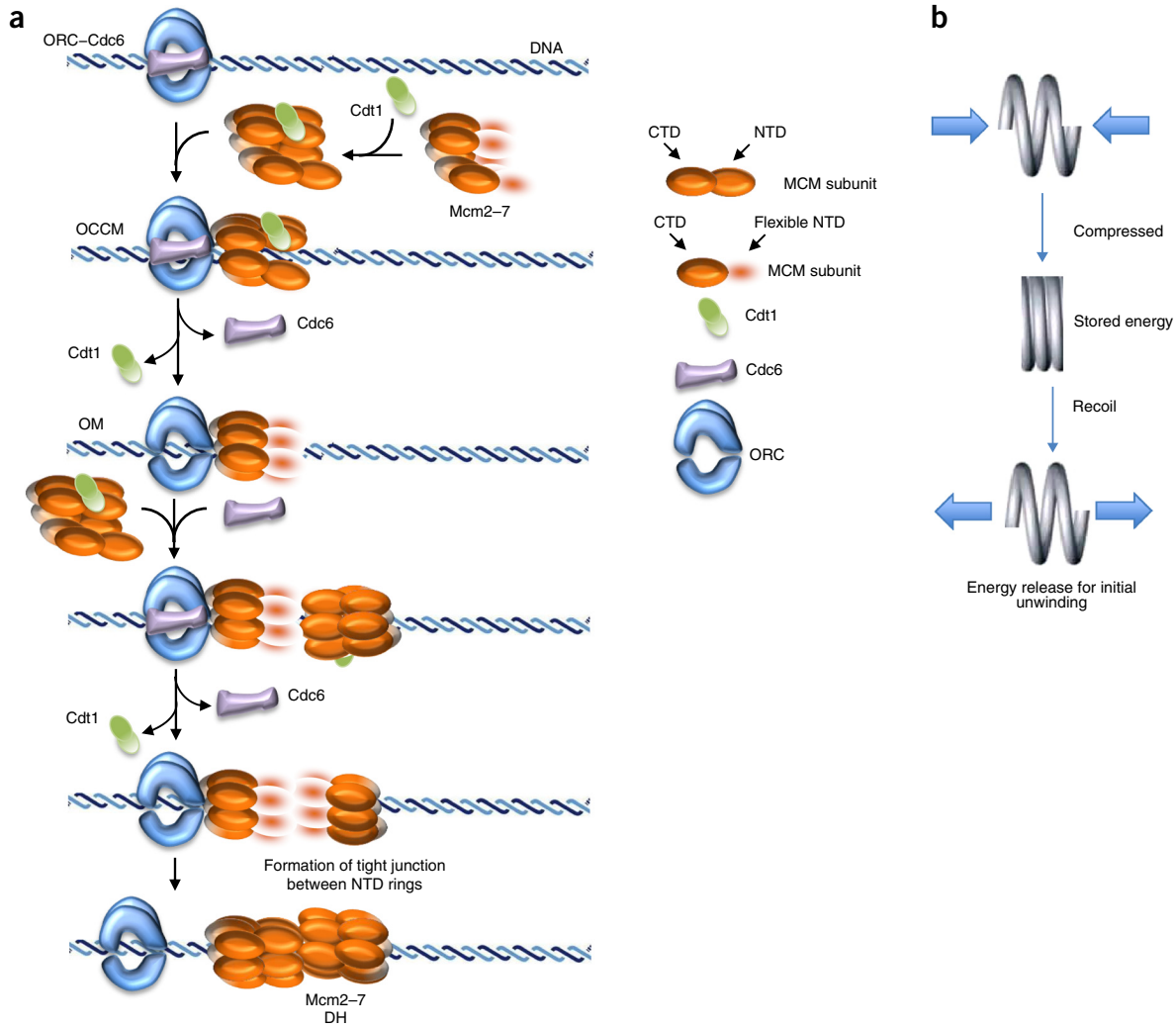

Figure 6 Models for loading and translocation of Mcm2–7 inspired by its coiled structure. (**a**) Cdt1 binds and stabilizes the NTDs of the Mcm2–7 complex before it is recruited to origin DNA by ORC–Cdc6 to form OCCM. During this process, conformational changes occur in the Mcm2–7 structure that widen the Mcm2-Mcm5 gate and remove the WH of Mcm5 from the central channel. After ATP hydrolysis, Cdc6 and Cdt1 are released sequentially, leaving ORC–MCM (OM) at the origin, with the CTDs of MCM subunits forming a ring and the NTDs less ordered; this aids in recruitment of the second Cdt1–MCM complex. Again, the release of Cdt1 destabilizes the NTDs of MCM to facilitate the formation the tight junctions of the DH. (**b**) The compression of two MCM coils to form the planar DH ring is an energy-requiring process. Stored energy in the constrained DH ring is used for the initial melting of duplex DNA upon uncoupling of the DH.

closed-ring configuration. Establishing the open coil as the ground state of the MCM hexamer has profound implications for the DNA-replication mechanism during both initiation and elongation.

First, upon activation of the DH, energy stored in the planar rings will be unleashed to provide the mechanical energy to uncouple the DH as each SH springs open to allow the escape of the melted single-stranded DNAs through the narrow Mcm2-Mcm5 gate to opposite sides. It is not clear whether ATP hydrolysis by MCM is required for separation of the DH, but the two Mcm2-Mcm5 interfaces are exactly arranged on opposite sides of the DH[15,16] to facilitate this process. Second, the open-coil structure of the Mcm2–7 hexamer may determine the mode of action of the CMG helicase in its translocation along single-stranded DNA during DNA unwinding. We believe that this action of the CMG helicase may be driven by the repeated spring action of the open coil in a manner consistent with an inchworm motion (**Supplementary Video 2**). We note that a similar spring-action mechanism has been proposed for the T7 gp4 hexameric replicative helicase[59].

One prediction related to the notion of a spring action rather than a pumpjack mechanism[39] in DNA unwinding is that an open-ring intermediate should be observed in the CMG structure. Another is that the binding of ATP is required for the formation of the planar ring when energy is stored, and that hydrolysis of ATP enables conformational cycling from the ring to the coil conformation. In fact, this prediction is consistent with the recent cryo-EM maps of the CMGs from both yeast and flies[39,55], in which one conformer of CMG has a gap between Mcm2 and Mcm5 (**Supplementary Fig. 7e–g**). Supporting evidence for the second prediction could be found in the *Drosophila* CMG structure[38,55,58], in which binding of an ATP analog (ADP-BeF_3 or ATP-γS) favors the planar conformation. The axial displacement of the interior loops of the MCM subunits during the transition from coil to planar conformation could be 15–20 Å (**Supplementary Video 1**), which would translate into a step size of the spring as large as 5–7 nt. This hypothetical step size is much larger than the 2–3 nt proposed for T7 helicase, DnaB and *Drosophila* CMG[55,59,60]. It is quite possible that Cdc45–GINS acts as a latch that limits the stride of the spring

(**Supplementary Video 2**). Ultimately, to determine the mechanism of ATP-hydrolysis-driven translocation of the catalytic MCM core, researchers will need high-resolution structures of the CMG helicase or the replisome in different functional states that will enable them to distinguish the identity of bound nucleotides at each ATPase center.

METHODS

Methods, including statements of data availability and any associated accession codes and references, are available in the online version of the paper.

Note: Any Supplementary Information and Source Data files are available in the online version of the paper.

ACKNOWLEDGMENTS

We thank the Tsinghua University Branch of the China National Center for Protein Sciences (Beijing, China) for technical support with cryo-EM data collection and for computation resources. Part of the computation was done on the Computing Platform of the Center for Life Science, Peking University. We also thank J. Diffley and S. Gasser (Francis Crick Institute, London, UK) for yeast and *E. coli* strains. This work was supported by the Ministry of Science and Technology of China (grants 2013CB910404 and 2016YFA0500700 to N.G.), the National Natural Science Foundation of China (grants 31422016, 31470722 and 31630087 to N.G.), the Research Grants Council of Hong Kong (grants GRF16138716 to B.-K.T.; GRF664013, HKUST12/CRF/13G, GRF16104115 and GRF16143016 to Y.Z. and B.-K.T.; and IGN15SC02 to Y.Z.). N.L. is supported by a postdoctoral fellowship from the Peking-Tsinghua Center for Life Sciences.

AUTHOR CONTRIBUTIONS

Y.Z. and P.Y.K.Y. purified proteins; E.C., H.W. and N.L. collected and processed data; P.Y.K.Y., Y.Z. and E.C. generated animations; and Y.Z., E.C., N.G. and B.-K.T. prepared the manuscript.

COMPETING FINANCIAL INTERESTS

The authors declare no competing financial interests.

1. Zhu, W., Abbas, T. & Dutta, A. DNA replication and genomic instability. *Adv. Exp. Med. Biol.* **570**, 249–279 (2005).
2. O'Donnell, M., Langston, L. & Stillman, B. Principles and concepts of DNA replication in bacteria, archaea, and eukarya. *Cold Spring Harb. Perspect. Biol.* **5**, a010108 (2013).
3. Bell, S.P. & Labib, K. Chromosome duplication in *Saccharomyces cerevisiae*. *Genetics* **203**, 1027–1067 (2016).
4. Tanaka, S. & Diffley, J.F. Interdependent nuclear accumulation of budding yeast Cdt1 and Mcm2-7 during G1 phase. *Nat. Cell Biol.* **4**, 198–207 (2002).
5. Tye, B.K. MCM proteins in DNA replication. *Annu. Rev. Biochem.* **68**, 649–686 (1999).
6. Bochman, M.L. & Schwacha, A. The Mcm complex: unwinding the mechanism of a replicative helicase. *Microbiol. Mol. Biol. Rev.* **73**, 652–683 (2009).
7. Bell, S.D. & Botchan, M.R. The minichromosome maintenance replicative helicase. *Cold Spring Harb. Perspect. Biol.* **5**, a012807 (2013).
8. Remus, D. *et al.* Concerted loading of Mcm2-7 double hexamers around DNA during DNA replication origin licensing. *Cell* **139**, 719–730 (2009).
9. Evrin, C. *et al.* A double-hexameric MCM2-7 complex is loaded onto origin DNA during licensing of eukaryotic DNA replication. *Proc. Natl. Acad. Sci. USA* **106**, 20240–20245 (2009).
10. Costa, A., Hood, I.V. & Berger, J.M. Mechanisms for initiating cellular DNA replication. *Annu. Rev. Biochem.* **82**, 25–54 (2013).
11. Frigola, J., Remus, D., Mehanna, A. & Diffley, J.F. ATPase-dependent quality control of DNA replication origin licensing. *Nature* **495**, 339–343 (2013).
12. Fernández-Cid, A. *et al.* An ORC/Cdc6/MCM2-7 complex is formed in a multistep reaction to serve as a platform for MCM double-hexamer assembly. *Mol. Cell* **50**, 577–588 (2013).
13. Sun, J. *et al.* Cryo-EM structure of a helicase loading intermediate containing ORC–Cdc6–Cdt1–MCM2-7 bound to DNA. *Nat. Struct. Mol. Biol.* **20**, 944–951 (2013).
14. Ticau, S., Friedman, L.J., Ivica, N.A., Gelles, J. & Bell, S.P. Single-molecule studies of origin licensing reveal mechanisms ensuring bidirectional helicase loading. *Cell* **161**, 513–525 (2015).
15. Sun, J. *et al.* Structural and mechanistic insights into Mcm2-7 double-hexamer assembly and function. *Genes Dev.* **28**, 2291–2303 (2014).
16. Li, N. *et al.* Structure of the eukaryotic MCM complex at 3.8 Å. *Nature* **524**, 186–191 (2015).
17. Heller, R.C. *et al.* Eukaryotic origin-dependent DNA replication in vitro reveals sequential action of DDK and S-CDK kinases. *Cell* **146**, 80–91 (2011).
18. Yeeles, J.T., Deegan, T.D., Janska, A., Early, A. & Diffley, J.F. Regulated eukaryotic DNA replication origin firing with purified proteins. *Nature* **519**, 431–435 (2015).
19. Labib, K. How do Cdc7 and cyclin-dependent kinases trigger the initiation of chromosome replication in eukaryotic cells? *Genes Dev.* **24**, 1208–1219 (2010).
20. Sheu, Y.J. & Stillman, B. Cdc7-Dbf4 phosphorylates MCM proteins via a docking site-mediated mechanism to promote S phase progression. *Mol. Cell* **24**, 101–113 (2006).
21. Francis, L.I., Randell, J.C., Takara, T.J., Uchima, L. & Bell, S.P. Incorporation into the prereplicative complex activates the Mcm2-7 helicase for Cdc7-Dbf4 phosphorylation. *Genes Dev.* **23**, 643–654 (2009).
22. Deegan, T.D., Yeeles, J.T. & Diffley, J.F. Phosphopeptide binding by Sld3 links Dbf4-dependent kinase to MCM replicative helicase activation. *EMBO J.* **35**, 961–973 (2016).
23. Tanaka, S., Nakato, R., Katou, Y., Shirahige, K. & Araki, H. Origin association of Sld3, Sld7, and Cdc45 proteins is a key step for determination of origin-firing timing. *Curr. Biol.* **21**, 2055–2063 (2011).
24. Zegerman, P. & Diffley, J.F. Phosphorylation of Sld2 and Sld3 by cyclin-dependent kinases promotes DNA replication in budding yeast. *Nature* **445**, 281–285 (2007).
25. Tanaka, S. *et al.* CDK-dependent phosphorylation of Sld2 and Sld3 initiates DNA replication in budding yeast. *Nature* **445**, 328–332 (2007).
26. Tanaka, S. & Araki, H. Helicase activation and establishment of replication forks at chromosomal origins of replication. *Cold Spring Harb. Perspect. Biol.* **5**, a010371 (2013).
27. Muramatsu, S., Hirai, K., Tak, Y.S., Kamimura, Y. & Araki, H. CDK-dependent complex formation between replication proteins Dpb11, Sld2, Pol (epsilon, and GINS in budding yeast. *Genes Dev.* **24**, 602–612 (2010).
28. Fu, Y.V. *et al.* Selective bypass of a lagging strand roadblock by the eukaryotic replicative DNA helicase. *Cell* **146**, 931–941 (2011).
29. Samel, S.A. *et al.* A unique DNA entry gate serves for regulated loading of the eukaryotic replicative helicase MCM2-7 onto DNA. *Genes Dev.* **28**, 1653–1666 (2014).
30. Takara, T.J. & Bell, S.P. Multiple Cdt1 molecules act at each origin to load replication-competent Mcm2-7 helicases. *EMBO J.* **30**, 4885–4896 (2011).
31. Riera, A., Tognetti, S. & Speck, C. Helicase loading: how to build a MCM2-7 double-hexamer. *Semin. Cell Dev. Biol.* **30**, 104–109 (2014).
32. Coster, G., Frigola, J., Beuron, F., Morris, E.P. & Diffley, J.F. Origin licensing requires ATP binding and hydrolysis by the MCM replicative helicase. *Mol. Cell* **55**, 666–677 (2014).
33. Kang, S., Warner, M.D. & Bell, S.P. Multiple functions for Mcm2-7 ATPase motifs during replication initiation. *Mol. Cell* **55**, 655–665 (2014).
34. Miller, J.M. & Enemark, E.J. Archaeal MCM proteins as an analog for the eukaryotic Mcm2-7 helicase to reveal essential features of structure and function. *Archaea* **2015**, 305497 (2015).
35. Chong, J.P., Hayashi, M.K., Simon, M.N., Xu, R.M. & Stillman, B. A double-hexamer archaeal minichromosome maintenance protein is an ATP-dependent DNA helicase. *Proc. Natl. Acad. Sci. USA* **97**, 1530–1535 (2000).
36. Slaymaker, I.M. & Chen, X.S. MCM structure and mechanics: what we have learned from archaeal MCM. *Subcell. Biochem.* **62**, 89–111 (2012).
37. Lyubimov, A.Y., Costa, A., Bleichert, F., Botchan, M.R. & Berger, J.M. ATP-dependent conformational dynamics underlie the functional asymmetry of the replicative helicase from a minimalist eukaryote. *Proc. Natl. Acad. Sci. USA* **109**, 11999–12004 (2012).
38. Costa, A. *et al.* The structural basis for MCM2-7 helicase activation by GINS and Cdc45. *Nat. Struct. Mol. Biol.* **18**, 471–477 (2011).
39. Yuan, Z. *et al.* Structure of the eukaryotic replicative CMG helicase suggests a pumpjack motion for translocation. *Nat. Struct. Mol. Biol.* **23**, 217–224 (2016).
40. Wu, R., Wang, J. & Liang, C. Cdt1p, through its interaction with Mcm6p, is required for the formation, nuclear accumulation and chromatin loading of the MCM complex. *J. Cell Sci.* **125**, 209–219 (2012).
41. Chen, S. & Bell, S.P. CDK prevents Mcm2-7 helicase loading by inhibiting Cdt1 interaction with Orc6. *Genes Dev.* **25**, 363–372 (2011).
42. Liu, C. *et al.* Structural insights into the Cdt1-mediated MCM2-7 chromatin loading. *Nucleic Acids Res.* **40**, 3208–3217 (2012).
43. Khayrutdinov, B.I. *et al.* Structure of the Cdt1 C-terminal domain: conservation of the winged helix fold in replication licensing factors. *Protein Sci.* **18**, 2252–2264 (2009).
44. Evrin, C. *et al.* The ORC/Cdc6/MCM2-7 complex facilitates MCM2-7 dimerization during prereplicative complex formation. *Nucleic Acids Res.* **42**, 2257–2269 (2014).
45. Bochman, M.L. & Schwacha, A. The Mcm2-7 complex has in vitro helicase activity. *Mol. Cell* **31**, 287–293 (2008).
46. Miller, J.M., Arachea, B.T., Epling, L.B. & Enemark, E.J. Analysis of the crystal structure of an active MCM hexamer. *eLife* **3**, e03433 (2014).
47. Froelich, C.A., Kang, S., Epling, L.B., Bell, S.P. & Enemark, E.J. A conserved MCM single-stranded DNA binding element is essential for replication initiation. *eLife* **3**, e01993 (2014).
48. Enemark, E.J. & Joshua-Tor, L. On helicases and other motor proteins. *Curr. Opin. Struct. Biol.* **18**, 243–257 (2008).

49. Lyubimov, A.Y., Strycharska, M. & Berger, J.M. The nuts and bolts of ring-translocase structure and mechanism. *Curr. Opin. Struct. Biol.* **21**, 240–248 (2011).
50. O'Shea, V.L. & Berger, J.M. Loading strategies of ring-shaped nucleic acid translocases and helicases. *Curr. Opin. Struct. Biol.* **25**, 16–24 (2014).
51. Arias-Palomo, E., O'Shea, V.L., Hood, I.V. & Berger, J.M. The bacterial DnaC helicase loader is a DnaB ring breaker. *Cell* **153**, 438–448 (2013).
52. Samson, R.Y., Abeyrathne, P.D. & Bell, S.D. Mechanism of archaeal MCM helicase recruitment to DNA replication origins. *Mol. Cell* **61**, 287–296 (2016).
53. Bowman, G.D., O'Donnell, M. & Kuriyan, J. Structural analysis of a eukaryotic sliding DNA clamp-clamp loader complex. *Nature* **429**, 724–730 (2004).
54. Yao, N.Y. & O'Donnell, M. The RFC clamp loader: structure and function. *Subcell. Biochem.* **62**, 259–279 (2012).
55. Abid Ali, F. *et al.* Cryo-EM structures of the eukaryotic replicative helicase bound to a translocation substrate. *Nat. Commun.* **7**, 10708 (2016).
56. Chen, S., de Vries, M.A. & Bell, S.P. Orc6 is required for dynamic recruitment of Cdt1 during repeated Mcm2-7 loading. *Genes Dev.* **21**, 2897–2907 (2007).
57. Bowers, J.L., Randell, J.C., Chen, S. & Bell, S.P. ATP hydrolysis by ORC catalyzes reiterative Mcm2-7 assembly at a defined origin of replication. *Mol. Cell* **16**, 967–978 (2004).
58. Costa, A. *et al.* DNA binding polarity, dimerization, and ATPase ring remodeling in the CMG helicase of the eukaryotic replisome. *eLife* **3**, e03273 (2014).
59. Syed, S., Pandey, M., Patel, S.S. & Ha, T. Single-molecule fluorescence reveals the unwinding stepping mechanism of replicative helicase. *Cell Rep.* **6**, 1037–1045 (2014).
60. Itsathitphaisarn, O., Wing, R.A., Eliason, W.K., Wang, J. & Steitz, T.A. The hexameric helicase DnaB adopts a nonplanar conformation during translocation. *Cell* **151**, 267–277 (2012).

ONLINE METHODS

Sample purification. We used yeast strains yJF38 and yJF39 (gifts from John Diffley, The Francis Crick Institute, UK) to express the Cdt1–Mcm2–7 heptamer and Mcm2–7 hexamer, respectively. Twenty liters of cells were grown in YP-raffinose at 30 °C to log phase to a cell density of 4×10^7 cells/ml before being arrested in G1 phase with 100 ng/ml of α-factor at 30 °C for 2 h. We induced overexpression of the complexes by adding galactose (final 2%) to the cell culture. The cells were collected after 3 h and washed with ice-cold water. Cell pellets were treated with lyticase in spheroplasting buffer before lysis in extraction buffer (50 mM HEPES/KOH, pH 7.5, 100 mM potassium glutamate, 10 mM magnesium acetate, 0.25% Triton X-100, 3 mM ATP, 1 mM dithiothreitol, 1 mM EDTA, and 1× protease inhibitor cocktail (Roche)). The lysates were then centrifuged three times for 20 min each time at 25,000*g*. The clear phase was recovered and subjected to anti-Flag immunoprecipitation of 3×Flag-Mcm3 with a 2.5-ml bed volume of anti-Flag M2 agarose (Sigma) at 4 °C for 3 h. Beads were recovered and washed extensively with wash buffer (50 mM HEPES/KOH, pH 7.5, 100 mM potassium glutamate, 8 mM magnesium chloride, 0.02% NP-40, 3 mM ATP, 1 mM EDTA, and 1× protease inhibitor cocktail). For elution we added 0.3 mg/ml (final concentration) 3×Flag peptide and incubated the beads at 4 °C for 25 min. The beads were washed once with an equal volume of wash buffer. Eluates were combined and concentrated using Amicon centrifugal filter concentrators (30-kDa molecular weight cutoff; Millipore). For the Mcm2–7 hexamer, the eluates were preincubated with IgG Sepharose 6 Fast Flow beads (GE Healthcare) at 4 °C for 1 h, to remove endogenous Cdt1. The concentrated complexes were then applied to the top of a 20–40% glycerol gradient in wash buffer with protease inhibitors. The gradients were centrifuged in a TLS-55 rotor (Beckman Optima TLX ultracentrifuge) at 175,000*g* for 6.5 h. The fractions were collected from the top of the gradient after centrifugation. The fractions containing the Cdt1–Mcm2–7 heptamers (or Mcm2–7 hexamers) were pooled and processed for electron microscopy analysis.

Grid preparation and data collection. The Mcm2–7 hexamer and Cdt1–Mcm2–7 heptamer were concentrated by ultrafiltration for buffer change to remove glycerol. To prepare the heptamer + AMPPNP and heptamer + ADP samples, we added 1 mM AMPPNP or ADP to the sample solution and incubated it for 1 h before cryo-grid preparation. Initially, grid preparation was done with holey carbon grids (Quantifoil). However, the samples tended to stay away from the holes and aggregate at the edge, making the data collection very inefficient. Preliminary analysis (from around 1,000 and 500 micrographs for the heptamer and hexamer samples, respectively) indicated a top-view orientation preference for both samples. In a previous cryo-EM study of a similar AAA+ hexamer (N-ethylmaleimide sensitive factor)[61], NP-40 was used to increase the occurrence of side-view particles. Our attempt to prepare cryo-grids with buffer containing varying concentrations of NP-40 (0.001%, 0.005% and 0.05%) did not result in substantial improvement of the distribution of particles into the holes, nor did it solve the orientation problem completely. We also attempted to replace copper grids with Quantifoil gold grids, but this yielded little improvement. Finally, we resorted to carbon-coated Quantifoil grids, which are known to compromise image contrast. Specifically, we applied 4-µl aliquots of sample to a glow-discharged holey carbon grid (Quantifoil R1.2/1.3) with a homemade continuous carbon film. For the hexamer–ADP sample, we added 1 mM ADP and 0.005% NP-40 to the sample solution and incubated it for 1 h before cryo-grid preparation. All grids were blotted for 1.5 s and flash-frozen in liquid ethane with an FEI Vitrobot Mark IV. Grids were examined with an FEI Titan Krios operated at 300 kV. Micrographs were collected with a K2 Summit detector (Gatan) in counting mode, at a nominal magnification of 22,500×, which yielded a pixel size of 1.32 Å at objective scale. Defocus values were set in a range from −2.0 to −3.0 µm. All images were recorded with UCSFImage4 (http://cryoem.ucsf.edu/software/UCSFImage.html), a semi-automated low-dose data-collection program. Each micrograph was dose-fractionated to 32 frames, with a dose rate of 8.2 counts (10.9 electrons) per physical pixel per second for an exposure time of 8 s.

Image processing. For cryo-EM data, we corrected original image stacks for drift and beam-induced motion at the micrograph level by using MotionCorr[62]. We used SPIDER[63] and RELION[64] for micrograph screening, automatic particle-picking, and normalization. Contrast-transfer-function parameters were estimated with CTFFIND3 (ref. 65). 2D and 3D classification and refinement were done with RELION. For the heptamer + AMPPNP sample, a total of 402,000 raw particles (with a binning factor of two) from 2,191 micrographs were subjected to reference-free 2D classification (**Supplementary Fig. 1e**,**f**). After the 2D-classification-based particle screening, 244,400 particles were subjected to 3D classification. The reference for 3D classification was converted from the Mcm2–7 DH model (PDB 3JA8)[16] and filtered to 40 Å. After 3D classification, 63,000 particles were assigned to the heptamer–AMPPNP complex, and 51,800 particles were assigned to the hexamer–AMPPNP complex. These two groups of particles were then subjected to reference-based refinement. The maps were further processed with the post-processing options of RELION with a *B* factor of −200 Å, and the modulation transfer function of the detector was also corrected. The final resolutions of the heptamer–AMPPNP complex and hexamer–AMPPNP complex were 7.1 Å and 8.0 Å (gold-standard FSC 0.143 criteria), respectively (**Supplementary Fig. 2b**–**f**). The heptamer + ADP and hexamer + ADP + NP-40 data sets were processed similarly as described above (**Table 1**). The final resolutions of the heptamer–ADP complex and the hexamer–ADP complex from the heptamer + ADP data set were 7.1 Å and 8.0 Å (gold-standard FSC 0.143 criteria), respectively (**Table 1**). The final resolution of the hexamer–ADP complex from the hexamer + ADP + NP-40 data set was 7.3 Å. The final density map of the hexamer–ADP complex from the heptamer + ADP data set was very similar to the one from the hexamer + ADP + NP40 data set, and the one with higher resolution was used for structural analysis (**Table 1**).

Model building. We carried out manual model docking based on rigid domains using UCSF Chimera[66]. The six CTD-As and six NTDs of Mcm2–7 (PDB 3JA8) were docked as 12 rigid bodies. The sequence of the yeast Cdt1 was subjected to 2D structure prediction with PSIPRED[67]. On the basis of the results of 2D prediction, Cdt1 can be divided into three domains: NTD, MD and CTD. We subjected these three domains of Cdt1 and the CTEs of Mcm4, Mcm5 and Mcm6 to 3D structure prediction with I-TASSER[68]. For the model prediction, we used previously characterized structures of mouse and human Cdt1 C-terminal fragments (PDB 2ZXX, PDB 2WVR, PDB 2KLO, PDB 3A4C and PDB 2RQQ)[43,69–71] as templates for the CTD and MD of yeast Cdt1, and previous NMR spectroscopy structures of the C-terminal WH domain of archaeal MCMs (PDB 2MA3 and PDB 2M45)[72] as templates for the yeast MCM CTEs. Predicted models of Cdt1 were also docked as individual rigid bodies. Because of the limited resolution, only the backbone of the resulting Cdt1–Mcm2–7 model was refined in real space with the phenix.real_space_refine module[73] in the Phenix package[74], with rotamer restraints, Ramachandran plot restraints, C-β deviation restraints, secondary-structure restraints and reference-model restraints enabled. Models of the other nucleotide-saturated states were similarly refined. Figures and videos were generated using UCSF Chimera.

Data availability. The cryo-EM density maps have been deposited in the EMDB with accession numbers EMD-6671 (Cdt1–Mcm2–7–AMPPNP), EMD-6672 (Cdt1–Mcm2–7–ADP), EMD-6673 (Mcm2–7–AMPPNP) and EMD-6674 (Mcm2–7–ADP). The fitted atomic model of Cdt1–Mcm2–7–AMPPNP has been deposited in the PDB with accession number 5H7I. All other relevant data are available from the corresponding author on request.

61. Zhao, M. *et al.* Mechanistic insights into the recycling machine of the SNARE complex. *Nature* **518**, 61–67 (2015).
62. Li, X. *et al.* Electron counting and beam-induced motion correction enable near-atomic-resolution single-particle cryo-EM. *Nat. Methods* **10**, 584–590 (2013).
63. Shaikh, T.R. *et al.* SPIDER image processing for single-particle reconstruction of biological macromolecules from electron micrographs. *Nat. Protoc.* **3**, 1941–1974 (2008).
64. Scheres, S.H. RELION: implementation of a Bayesian approach to cryo-EM structure determination. *J. Struct. Biol.* **180**, 519–530 (2012).
65. Mindell, J.A. & Grigorieff, N. Accurate determination of local defocus and specimen tilt in electron microscopy. *J. Struct. Biol.* **142**, 334–347 (2003).
66. Pettersen, E.F. *et al.* UCSF Chimera—a visualization system for exploratory research and analysis. *J. Comput. Chem.* **25**, 1605–1612 (2004).
67. Buchan, D.W., Minneci, F., Nugent, T.C., Bryson, K. & Jones, D.T. Scalable web services for the PSIPRED Protein Analysis Workbench. *Nucleic Acids Res.* **41**, W349–W357 (2013).
68. Yang, J. *et al.* The I-TASSER Suite: protein structure and function prediction. *Nat. Methods* **12**, 7–8 (2015).
69. Lee, C. *et al.* Structural basis for inhibition of the replication licensing factor Cdt1 by geminin. *Nature* **430**, 913–917 (2004).

doi:10.1038/nsmb.3374

70. De Marco, V. *et al.* Quaternary structure of the human Cdt1-Geminin complex regulates DNA replication licensing. *Proc. Natl. Acad. Sci. USA* **106**, 19807–19812 (2009).
71. Jee, J. *et al.* Structure and mutagenesis studies of the C-terminal region of licensing factor Cdt1 enable the identification of key residues for binding to replicative helicase Mcm proteins. *J. Biol. Chem.* **285**, 15931–15940 (2010).
72. Wiedemann, C. *et al.* Structure and regulatory role of the C-terminal winged helix domain of the archaeal minichromosome maintenance complex. *Nucleic Acids Res.* **43**, 2958–2967 (2015).
73. Afonine, P.V. *et al.* Towards automated crystallographic structure refinement with phenix.refine. *Acta Crystallogr. D Biol. Crystallogr.* **68**, 352–367 (2012).
74. Adams, P.D. *et al.* PHENIX: a comprehensive Python-based system for macromolecular structure solution. *Acta Crystallogr. D Biol. Crystallogr.* **66**, 213–221 (2010).